Biochemistry

pubs.acs.org/biochemistry Article

Substrate Substitution in Kanosamine Biosynthesis Using Phosphonates and Phosphite Rescue

Natasha D. Vetter and David R. J. Palmer*

Cite This: *Biochemistry* 2021, 60, 1926−1932 Read Online

ACCESS | Metrics & More | Article Recommendations | Supporting Information

ABSTRACT: Kanosamine is an antibiotic and antifungal compound synthesized from glucose 6-phosphate (G6P) in *Bacillus subtilis* by the action of three enzymes: NtdC, which catalyzes NAD-dependent oxidation of the C3-hydroxyl; NtdA, a PLP-dependent aminotransferase; and NtdB, a phosphatase. We previously demonstrated that NtdC can also oxidize substrates such as glucose and xylose, though at much lower rates, suggesting that the phosphoryloxymethylene moiety of the substrate is critical for effective catalysis. To probe this, we synthesized two phosphonate analogues of G6P in which the bridging oxygen is replaced by methylene and difluoromethylene groups. These analogues are substrates for NtdC, with second-order rate constants an order of magnitude lower than those for G6P. NtdA converts the resulting 3-keto products to the corresponding kanosamine 6-phosphonate analogues. We compared the rates to the rate of NtdC oxidation of glucose and xylose and showed that the low reactivity of xylose could be rescued 4-fold by the presence of phosphite, mimicking G6P in two pieces. These results allow the evaluation of the individual energetic contributions to catalysis of the bridging oxygen, the bridging C6 methylene, the phosphodianion, and the entropic gain of one substrate versus two substrate pieces. Phosphite also rescued the reversible formation 3-amino-3-deoxy-D-xylose by NtdA, demonstrating that truncated and nonhydrolyzable analogues of kanosamine 6-phosphate can be generated enzymatically.

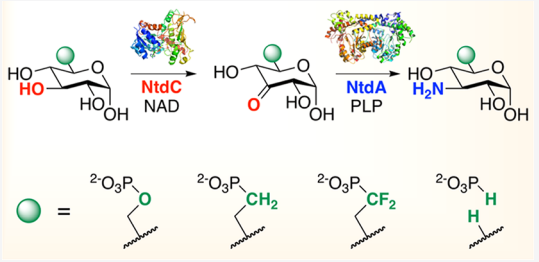

Kanosamine, 3-amino-3-deoxy-D-glucose, is an amino sugar known to inhibit the growth of a variety of pathogenic bacterial species, including *Staphylococcus aureus*, as well as certain fungi such as *Candida* spp. Inhibition of these organisms by kanosamine is a result of intracellular phosphorylation to kanosamine 6-phosphate (K6P), which then inhibits glucosamine-6-phosphate synthase during cell wall synthesis.[1,2] Kanosamine is also a precursor to more complex natural products and antibiotics, such as kanamycin, rifamycins, and ansamycins.[1,3,4]

A variety of *Bacillus* species have been shown to produce kanosamine[3−6] and, as a result, have found utility in the treatment of plant disease.[1,7] Kanosamine was first isolated from cultures of *Bacillus pumilis* in 1968[5] and later from *Bacillus cereus*.[1,6] The proposed biosynthetic pathway of kanosamine from these species involves first the C3 oxidation of UDP-glucose by a dehydrogenase, then transamination using a PLP-dependent aminotransferase, and hydrolysis of the UDP at C1. We have more recently demonstrated that in *Bacillus subtilis*, this pathway starts not with UDP-glucose but rather with glucose 6-phosphate (G6P) (Figure 1A). The final step catalyzed by NtdB, a phosphatase, irreversibly cleaves the C6 phosphate group. This was the first time the functions of these enzymes and this pathway were demonstrated unambiguously.[8,9] Prior to that work, these three enzymes were mistakenly believed to make 3,3′-neotrehalosadiamine, resulting in the *ntd* designation. We have since examined

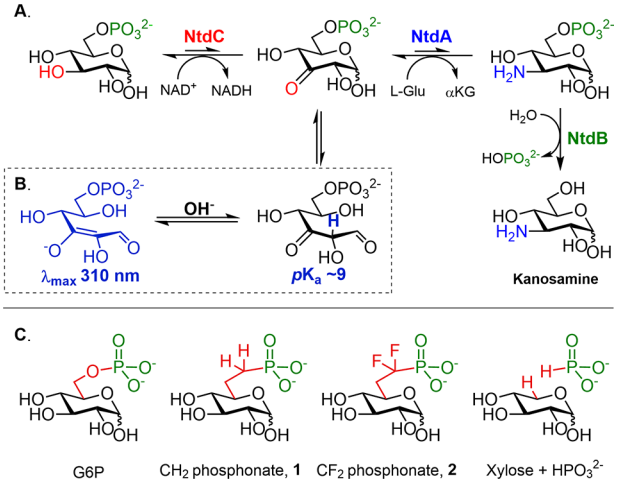

Figure 1. (A) Kanosamine biosynthesis in *B. subtilis*. (B) Enolate formation from 3oG6P. (C) Structures of G6P, phosphonate analogues of G6P, and xylose and inorganic phosphite mimicking G6P in two pieces.

Received: April 23, 2021
Revised: June 1, 2021
Published: June 7, 2021

similar enzymes from *B. cereus* UW85 (KabABC) and have shown that they have the same enzymatic functions as NtdABC.[10]

The first step in this pathway catalyzed by NtdC, a G6P 3-dehydrogenase, oxidizes the C3 hydroxyl of G6P to generate a unique 3-keto reducing sugar. This product, 3-oxo-G6P (3oG6P), is only one of very few examples of known biologically relevant 3-keto sugars.[11−14] In solution, G6P and 3oG6P rapidly undergo mutarotation, and therefore as a result, 3oG6P transiently exists in the open-chain form as a 1,3-dicarbonyl, which is then deprotonated at C2 under alkaline conditions to give the enolate form shown in Figure 1B, producing a strong, characteristic ultraviolet (UV) absorbance at 310 nm.[8,15] We recently demonstrated a carbocyclic analogue of the α-anomer of G6P was a substrate for NtdC, and the resulting product, which is incapable of the ring opening and enolization shown in Figure 1B, can act as a substrate for NtdA.[16] This confirmed all previous observations and established that these two enzymes had co-evolved so that both process the α-anomer, avoiding the observed side reactions associated with ring opening that would be required for mutarotation.

Having observed that NtdC and NtdA can accept a non-natural sugar as a substrate, we chose to investigate whether other substrate analogues could be accepted into the active sites of these enzymes. Our previous work with the Ntd enzymes showed that the C6 phosphate group of the substrate is crucial for the proper activity of the enzyme, with both glucose and xylose displaying only minimal activity with the enzyme. John Richard's laboratory has shown that the low activity of several enzymes with truncated substrates can be rescued with the addition of various dianions, mimicking the substrate in pieces.[17−20] Here we describe the ability of NtdC to catalyze the oxidation of G6P analogues in which the C6-phosphate group has been replaced by a nonhydrolyzable methylenephosphonate or difluoromethylenephosphonate group, or removed and rescued by the presence of phosphite (Figure 1C), and the energetic contributions of the substituted groups to catalysis. We also show that these non-natural substrates can be converted to the corresponding 3-amino-3-deoxy analogues by NtdA.

RESULTS AND DISCUSSION

Synthesis of Phosphonates 1 and 2. We were able to synthesize the desired phosphonate analogues of G6P according to a published procedure with minor changes (Scheme 1).[21] Methyl tri-*O*-benzyl glucopyranoside **5** was synthesized easily in two steps from commercially available 4,6-*O*-benzylidene **3** as previously reported.[16] The resulting C6 hydroxyl was converted to triflate **6** in quantitative yield, followed by displacement with either diethyl methylphosphonate or diethyl difluoromethyl phosphonate to give the desired protected glucose phosphonate **7** or **8**, respectively. It is important to note that excess methyl or difluoromethyl phosphonate was difficult to remove by flash column chromatography, as it co-elutes with the product and could be removed by rotary evaporation only at higher temperatures under high vacuum for extended periods of time.

Final deprotection was achieved in three steps giving compounds **1** and **2** in 25% and 16% yields, respectively. The loss of yield after deprotection is likely due to decomposition of the product during the acidic cleavage of the methyl glycoside, as well as difficulties in purifying the final

Scheme 1. Synthesis of Phosphonates 1 and 2

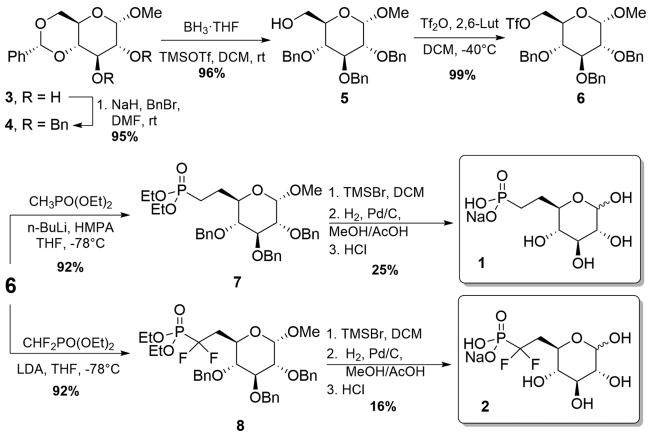

product. Several alternate deprotection attempts did not improve yields. For example, TMSI is reported to cleave the alkyl protecting groups of phosphonates much more rapidly than TMSBr,[22−24] and while this was the case, we also observed partial deprotection of the benzyl groups and substitution at the anomeric position. Regardless of the excess of TMSI used, a complex mixture was always obtained, which could not be resolved. Final products were purified by flash chromatography followed by ion exchange chromatography and converted to the monosodium salt by careful titration with acidic DOWEX, as our experience has shown that the monosodium salt is easier to handle and less hygroscopic than the free acid.

Activity of the NtdC-Catalyzed Reaction with Phosphonates 1 and 2. Initial assays with NtdC and NAD revealed that both methylene- and difluoromethylenephosphonate derivatives **1** and **2** were good substrates for the enzyme. Observation of the complete UV spectra evolving over time revealed two peaks corresponding to formation of both NADH (340 nm) and enolate (310 nm) (Figure 2A−C), similar to what is observed with G6P.[8,15] When the reaction mixture was supplemented with excess L-glutamate and the next enzyme in the pathway, NtdA, only NADH production was observed, while the 310 nm peak was no longer observed (Figure 2D−F). This indicates that NtdA could consume the 3-keto phosphonate products, converting them to the corresponding kanosamine phosphonates. Additionally, the apparent rate of the NtdC reaction with **1** and **2** was enhanced in the presence of NtdA, as was previously observed for the reaction with G6P,[8,15] but not to the same extent, suggesting NtdA is not as tolerant of the phosphonate analogues of 3oG6P.

The kinetics of **1** and **2** with NtdC was examined in detail by varying the concentrations of both substrates. Because of the overlapping peaks that evolve in the UV spectra over time, spectra were deconvoluted using a procedure developed previously to obtain kinetic information about both the NtdC reaction and enolate formation.[15] A complete kinetic profile of the enzyme with these substrates was obtained by varying the substrate concentration at different fixed concentrations of the second substrate, NAD (Figure 3). Kinetic parameters are summarized in Table 1 and compared to those of G6P.[15]

Both **1** and **2** were shown to be good substrates for NtdC, with k_{cat} values 4- and 12-fold lower than for G6P, respectively. The K_m parameter for **2** was on the same order of magnitude compared to that of G6P, while that of **1** was 3-fold higher.

https://doi.org/10.1021/acs.biochem.1c00283
Biochemistry 2021, 60, 1926−1932

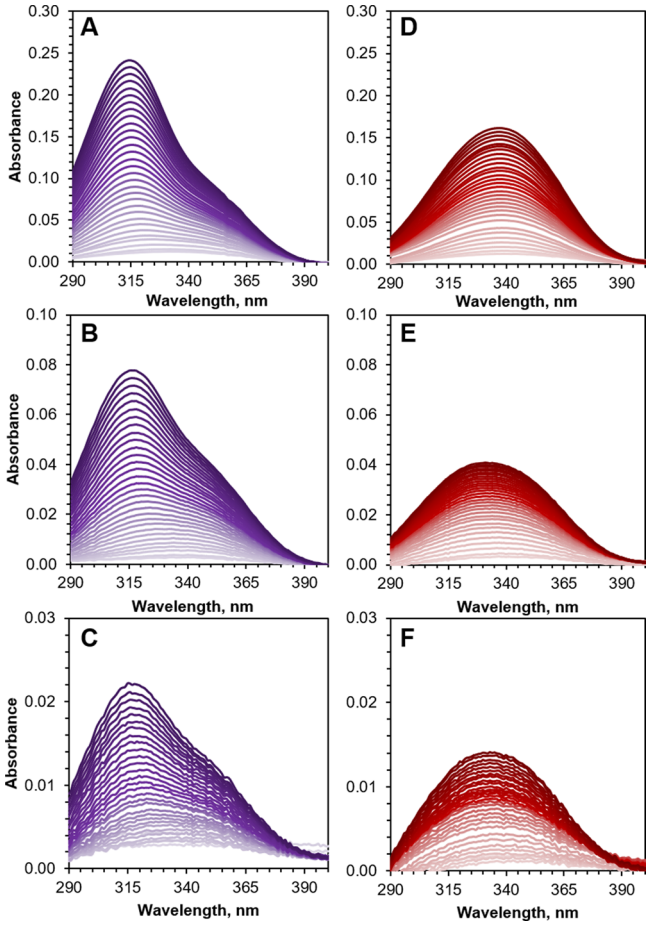

Figure 2. Wavelength traces of the reaction of NtdC with (A) G6P, (B) phosphonate **1**, and (C) phosphonate **2**. (D−F) Same reactions as in panels A−C, respectively, coupled to excess NtdA. All reactions were carried out at 25 °C in 100 mM AMP-HCl (pH 9.5) with 1 mM substrate, 1 mM NAD, and 10 mM L-glutamate.

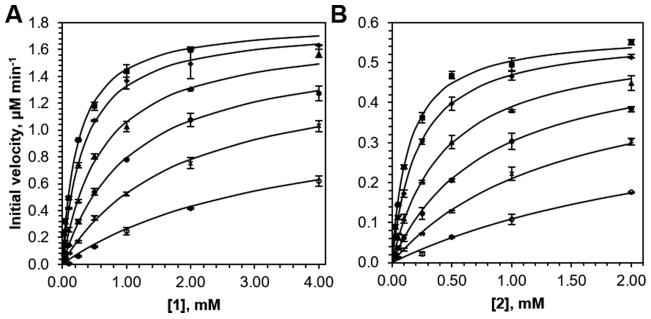

Figure 3. Saturation curves of the reaction of NtdC with (A) **1** and (B) **2**. All reactions were carried out at 25 °C in 100 mM AMP-HCl (pH 9.5), 28 nM NtdC, and fixed NAD concentrations of 5.00 (■), 2.50 (◆), 1.00 (▲), 0.50 (●), 0.25 (×), and 0.10 mM (○). All reactions were performed in duplicate.

This could indicate that hydrogen bonding of the phosphate-bridging group is important for properly binding and orienting the phosphate in the active site. Replacement of the oxygen atom with methylene and difluoromethylene groups will impact the pK_a of the substrate analogues. While G6P has a second pK_a value of 6.4, **1** has a value of 7.6, while **2** has a value of 5.6.[25] At the pH of the assay, all three substrates should exist predominantly as the dianion in solution, meaning the difference in pK_a should have a minimal effect on binding of the substrates. Carbon−fluorine bonds have a van der Waals radius of 1.47 Å, significantly larger than carbon−hydrogen bonds (1.2 Å); CF_2 cannot be considered a closely isosteric replacement for oxygen. The increased size of the bridging CF_2 compared to oxygen suggests that the active site has either adequate space or flexibility to accommodate changes in the substrate phosphate region. No change in the K_m of NAD was observed in the presence of either phosphonate compared to that of G6P. These results are similar to those of previous studies of yeast glucose-6-phosphate dehydrogenase (G6PDH) and 6-phosphogluconate dehydrogenase (6PGDH) with phosphonate analogues of their respective substrates. Both G6PDH and 6PGDH showed approximately 4-fold increases in the K_m of the phosphonate derivatives compared to those of their natural substrates, and no effect on the K_m of the cofactor. Additionally, G6PDH showed a 2-fold decrease in V_{max} while that of 6PGDH decreased 10-fold.[26,27] We have previously observed that with the natural substrate, G6P, NtdC follows a random bisubstrate mechanism, and kinetic isotope effect experiments revealed that the hydride transfer step is at least partially rate-limiting.[15] The observed decreases in the k_{cat} values suggest that hydride transfer is fully rate-limiting for these substrates.

Kinetics of Enolate Formation. The reactions of NtdC with **1** and **2** both showed the formation of a second peak in the UV spectra at 310 nm, characteristic of the non-enzymatic conversion of the 3-keto products to the corresponding enolates. We were able to measure both the enzymatic reaction and non-enzymatic enolate formation simultaneously, as we have previously done for 3oG6P formation,[15] by deconvolution of the wavelength traces evolving over the course of the reaction. From the deconvoluted peaks, plots of [NADH] versus A_{310} for the reaction with either phosphonate revealed extinction coefficients for the absorbing enolate species similar to that of 3oG6P (Table 1 and Figure S1A,B). Using the derived extinction coefficients, we were able to quantify both the absorbing enolate species and the non-absorbing 3-keto species throughout each reaction. Plots of the rate of enolate formation versus the steady state concentration of the non-absorbing 3-keto species revealed apparent rate constants of enolate formation, k_e, only marginally slower than that observed for 3oG6P (Table 1 and Figure S1C,D).

NtdC Activity with Smaller Monosaccharides. NtdC has been shown to be active in the presence of a small subset of monosaccharides, with the best substrates being G6P, glucose, and xylose.[8,28] While the enzyme has the greatest activity with G6P, glucose and xylose are <1% as active in comparison, which emphasizes the importance of the C6 phosphate on substrate binding and reactivity. We had therefore postulated that addition of either free phosphate or phosphite might rescue the low activity of glucose and xylose with NtdC. The addition of inorganic phosphate had no effect on the reaction with glucose or xylose; at high concentrations, slight inhibition was seen with glucose. In the presence of sodium phosphite, no effect was observed on the reaction with glucose; however, we were pleased to observe an increase in the rate of oxidation of xylose by NtdC. The apparent K_m of phosphite with xylose was found to be 27 ± 5 mM, which was calculated from a series of experiments in which the concentration of phosphite was varied, with fixed NAD and xylose concentrations [10 and 100 mM, respectively (Figure 4)].

https://doi.org/10.1021/acs.biochem.1c00283
Biochemistry 2021, 60, 1926−1932

Table 1. Kinetic Parameters of NtdC with 1 and 2

	G6P[a]	CH_2, **1**	CF_2, **2**
k_{cat} (s^{-1})	4.1 ± 0.1	1.08 ± 0.01	0.34 ± 0.01
K_m^{sugar} (mM)	0.043 ± 0.004	0.14 ± 0.01	0.065 ± 0.007
K_m^{NAD} (mM)	0.040 ± 0.004	0.05 ± 0.01	0.03 ± 0.01
K_i^{NAD} (mM)	0.9 ± 0.1	3.7 ± 0.4	6.0 ± 0.8
k_{cat}/K_m^{sugar}[b] (M^{-1} s^{-1})	$(9.6 \pm 0.8) \times 10^4$	$(7.7 \pm 0.6) \times 10^3$	$(5.3 \pm 0.5) \times 10^3$
k_{cat}/K_m^{NAD}[b] (M^{-1} s^{-1})	$(10 \pm 1) \times 10^4$	$(20 \pm 3) \times 10^3$	$(10 \pm 4) \times 10^3$
ε_{310}[c] (M^{-1} cm^{-1})	$(2.34 \pm 0.01) \times 10^4$	$(2.2 \pm 0.1) \times 10^4$	$(1.9 \pm 0.1) \times 10^4$
k_e[d] (s^{-1})	$(5.2 \pm 0.1) \times 10^{-3}$	$(3.3 \pm 0.1) \times 10^{-3}$	$(3.6 \pm 0.1) \times 10^{-3}$

[a]From ref 15. [b]Calculated from a global fitting of the kinetic data to eq S1 rearranged to treat V_{max}/K_a or V_{max}/K_b as a single parameter. [c]Calculated from eq S2. [d]Calculated from the pseudo-first-order rate equation (eq S3).

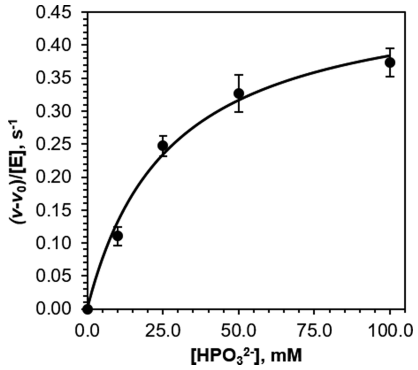

Figure 4. Estimation of the K_m of phosphite. All reactions were carried out in duplicate at 25 °C in 100 mM AMP-HCl (pH 9.5) with 100 mM xylose, 10 mM NAD, and 28 nM NtdC. Data were fit to the Michaelis–Menten equation (—).

We next examined the kinetics of NtdC in more detail by varying both xylose and phosphite concentrations, keeping the NAD concentration fixed under saturating conditions. We had observed that the maximum activity of the enzyme with xylose was obtained at 10 mM NAD, with some substrate inhibition at higher concentrations. Therefore, the apparent kinetic constants of NtdC with xylose were obtained at saturating NAD concentrations; the same experiments were then carried out in the presence of 10–100 mM phosphite, and the curves are shown in Figure 5A. The data for each curve were fit to the Michaelis–Menten equation to give apparent k_{cat} and K_m values, with the effect of phosphite concentration on these parameters shown in Figure 5B. The same data were also

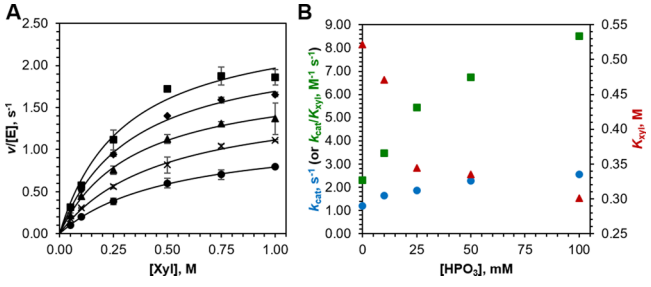

Figure 5. (A) Saturation curves of NtdC with xylose. Each experiment was carried out at 25 °C in 100 mM Amp-HCl (pH 9.5), 10 mM NAD, and 28 nM NtdC. The solid curves are the fits of the data to the Michaelis–Menten equation at 0 (●), 10 (×), 25 (▲), 50 (◆), and 100 mM (■) phosphite. (B) Effect of phosphite on the apparent kinetic parameters of NtdC with xylose from panel A: k_{cat} (●), K_m (▲), and k_{cat}/K_{Xyl} (■).

normalized to the initial velocities in the absence of phosphite, v_0 (Figure S2), fit to the equation describing a two-substrate mechanism (eq S4) to give the kinetic parameters listed in Table 2, and compared to those obtained in the absence of

Table 2. Kinetic Parameters of NtdC with Xylose and Phosphite

	0 mM Na_2HPO_3	10–100 mM Na_2HPO_3
k_{cat} (s^{-1})	1.2 ± 0.1	2.2 ± 0.1
k_{Xyl} (M)	0.52 ± 0.09	0.24 ± 0.03
k_{cat}/k_{Xyl} (M^{-1} s^{-1})	2.3 ± 0.2	9 ± 1
k_{HPO_3} (mM)	–	46 ± 5
$k_{cat}/k_{Xyl}k_{HPO_3}$ (M^{-2} s^{-1})	–	190 ± 30

phosphite. Examination of the kinetics of NtdC with xylose showed that in the presence of ≤100 mM phosphite, the K_m of xylose decreases by half, and the k_{cat} doubles, resulting in a nearly 4-fold increase in the second-order rate constant (Table 2 and Figure 5B). This indicates a 2-fold effect of phosphite, whereby both catalysis and substrate binding are enhanced.

We examined the coupled NtdC–NtdA reaction with xylose, in the same manner as with **1** and **2**; however, there was no observable effect of NtdA on the NtdC reaction. This is likely a result of the very slow turnover of the reaction of NtdC with xylose, such that any effect is too subtle to detect. The same was observed when we compared the rates of the uncoupled and coupled reactions in the presence of phosphite. Additionally, because very little enolate is visible in the reaction with xylose, we could not observe any activity by NtdA in the coupled reaction, so it was unclear if NtdA could accept oxidized xylose as a substrate.

While phosphite was shown to activate the reaction with xylose, we observed inhibition of the reaction with G6P. This is unsurprising because binding of phosphite in the active site would likely interfere with the binding of G6P. By varying both substrate concentrations at fixed phosphite concentrations, we were able to show that phosphite is a competitive inhibitor of both NAD and G6P [K_i = 20 ± 3 mM (Figure S3)], suggesting that it is capable of binding to both the phosphate binding region of the G6P binding site and the diphosphate binding region of the NAD binding site.

Our observations suggest that the size of the phosphate binding pocket is ideally spaced for the $CH_2OPO_3^{2-}$ of the sugar substrate, necessary for orienting the substrate properly in the active site for catalysis. The lack of any significant effect of phosphate with either glucose or xylose as the substrate suggests that inorganic phosphate is too sterically bulky to occupy this binding pocket while still allowing the sugar to

https://doi.org/10.1021/acs.biochem.1c00283
Biochemistry 2021, 60, 1926–1932

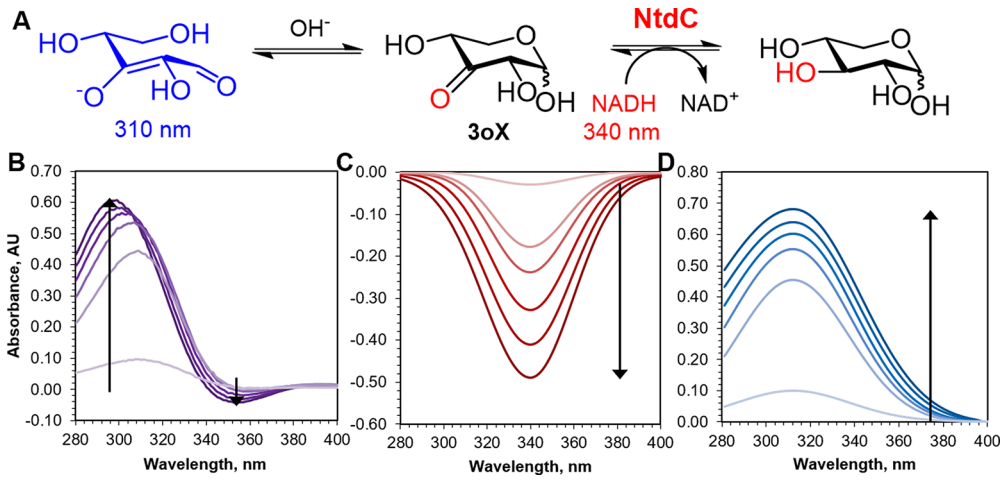

Figure 6. (A) Reaction of NtdC with **3oX** and NADH and simultaneous **3oX** enolate formation. (B) Wavelength traces of the reaction of NtdC with **3oX** and NADH. (C) Disappearance of NADH obtained by deconvolution of the wavelength traces in panel B. (C) Appearance of **3oX** enolate obtained by deconvolution of the wavelength traces in panel B. Arrows in panels B–D represent the direction of peak formation over time.

bind. The greater activity of glucose compared to that of xylose suggests that the CH_2OH is large enough to partially occupy the binding pocket of the phosphate and can satisfy some hydrogen bonding interactions. Xylose, however, has no moiety to occupy this site when bound in the reactive α-pyranose form, allowing phosphite to bind and satisfy many bonding interactions in the site, which consequently improves the catalytic efficiency and K_m.

Having shown that enzyme activity with xylose could be rescued with phosphite, we were interested to see if the same was true of substrates in the reverse direction with NtdC and NtdA. This prompted us to synthesize both 3-oxo-D-xylose [**3oX** (Figure 6A)] and 3-amino-3-deoxy-D-xylose [**3aX** (Figure 7A)]. We hypothesized that the lack of the C6 phosphate would cause **3oX** to be much more stable in solution than 3oG6P and allow us to assay both NtdC in the reverse direction and NtdA in the forward direction of the pathway.

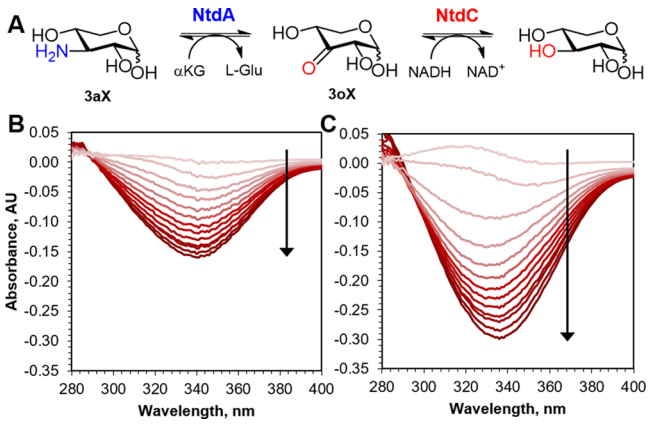

Figure 7. (A) Coupled NtdA–NtdC reaction with **3aX**, 2KG, and NADH. Wavelength traces of the reverse NtdA–NtdC reaction with **3aX** (B) without added phosphite and (C) with 100 mM phosphite. Reactions were carried out at 25 °C in 100 mM Tris-HCl (pH 8.0) with 0.25 M **3aX**, 5 mM 2KG, 0.2 mM NADH, 36 nM NtdC, and 0.18 μM NtdA over the course of 1 h. Arrows in panels B and C represent the direction of peak formation over time.

Activity of NtdA and NtdC with Xylose Analogues. Synthesis of both **3oX** and **3aX** followed similar synthetic routes that were seen for 3-oxo-D-glucose and kanosamine (Scheme S1),[3,8] and they were obtained in 37% (over four steps) and 23% (over six steps) yields, respectively. Aqueous, unbuffered solutions of **3oX** showed very little enolate formation at 310 nm, while in an alkaline solution, a prominent 310 nm peak was visible in the UV spectrum. This is similar to our previous observations with 3-oxoglucose, consistent with the non-enzymatic formation of the enolate species.[8] Our initial assays of **3oX** with NtdC in the presence of NADH showed the simultaneous disappearance of the 340 nm peak of NADH and the appearance of the 310 nm enolate peak (Figure 6). In the presence of 100 mM phosphite, the rate of NADH consumption was approximately 1.5 times faster, indicating that phosphite binding activates the reverse catalytic activity of NtdC. Additionally, the rate of enolate formation also nearly doubled. Quantification of the species in solution over the course of the reaction showed that approximately 70% of the reacted **3oX** is consumed by the NtdC reaction, while nearly 30% is being diverted to the unproductive enolate.

The NtdA–NtdC coupled reaction starting from **3aX**, NADH, and 2-ketoglutarate (2KG) resulted in the expected disappearance of NADH at 340 nm (Figure 7B), with very little enolate being formed, indicating that NtdA recognizes this substrate, and as expected, NtdC reduces the product, **3oX**. When the reaction mixture also included 100 mM phosphite, we observed an initial increase in absorbance at 310 nm and a 2-fold increase in the rate of NADH disappearance (Figure 7C), indicating that phosphite binding activates the transamination of **3aX** by NtdA also.

Effect of the C6 Bridging Group on Catalysis. The ability of phosphite to rescue low enzyme activity with small, truncated substrates has been observed with other enzymes, notably phosphoglucomutase (PGM),[29,30] G6P isomerase (PGI), G6P dehydrogenase (G6PDH), and 6-phosphogluconate dehydrogenase (6PGDH).[19,20] With PGM, a 1000-fold increase in the reaction rate is observed for smaller, truncated substrates, in the presence of phosphite. Work from Richard et al. has similarly postulated that phosphite binding interactions allow for the stabilization and activation of the enzyme compared to the unliganded catalyst that would otherwise exist

https://doi.org/10.1021/acs.biochem.1c00283
Biochemistry 2021, 60, 1926–1932

in an open, flexible, and inactive form. Their studies compare second-order rate constants of whole (phosphorylated) and truncated substrates to determine intrinsic binding energies. They have shown that the phosphate groups of the whole, natural substrates for PGI, G6PDH and 6PGDH, have intrinsic binding energies of 11−13 kcal/mol, 50% of which can be recovered by addition of phosphite for smaller, truncated substrates.[20]

In the case presented here, the second-order rate constants for NtdC-catalyzed oxidation can be used to approximate the relative activation barriers in the case of G6P ($\Delta G^{\ddagger}_{G6P}$), xylose ($\Delta G^{\ddagger}_{X}$), and xylose in the presence of phosphite ($\Delta G^{\ddagger}_{XP}$). Our results indicate that the phosphate of G6P accounts for approximately 6 kcal/mol of intrinsic binding energy ($\Delta G^{\ddagger}_{X} - \Delta G^{\ddagger}_{G6P}$) in the active site of NtdC, and with xylose, 2.6 kcal/mol (41%) is recovered in the presence of phosphite ($\Delta G^{\ddagger}_{X} - \Delta G^{\ddagger}_{XP}$) as shown in Figure 8. Much of the remaining binding

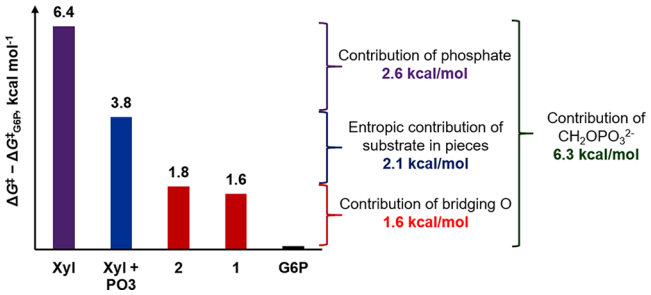

Figure 8. Contributions of substrate pieces to the intrinsic binding energy of G6P. Energies were calculated using second-order rate constants according to the equation $\Delta G^{\ddagger} = -RT \ln\left[\frac{k_{cat}}{K_m}\left(\frac{h}{\kappa_b T}\right)\right]$. For Xyl + PO_3, the third-order rate constant was used: $\Delta G^{\ddagger} = -RT \ln\left[\frac{k_{cat}}{K_m K_{HPO_3}}\left(\frac{h}{\kappa_b T}\right)\right]$.

energy may be identified as entropic contributions for a whole substrate compared to a substrate in pieces, and to lost interactions with the bridging CH_2OH. This is more evident upon comparison of the intrinsic binding energies of phosphonates **1** ($\Delta G^{\ddagger}_{1} - \Delta G^{\ddagger}_{G6P}$) and **2** ($\Delta G^{\ddagger}_{2} - \Delta G^{\ddagger}_{G6P}$), where 1.5−1.7 kcal/mol can be attributed to interactions, either electrostatic or steric, with the bridging oxygen alone, and is consistent with previous observations on G6PDH and 6PGDH.[26,27] This also suggests an approximately 2 kcal/mol advantage is gained from the binding of the whole substrate compared to the two substrate fragments ($\Delta G_{XP} - \Delta G_{1/2}$).[31] The estimated intrinsic binding energy of the phosphate is smaller than those observed for other enzymes, but this may be because the chemical step of the whole, natural substrate is not fully rate-limiting for NtdC.

CONCLUSION

We showed previously that NtdC, the enzyme that catalyzes the first step in kanosamine biosynthesis, can accept non-natural substrate analogues and that the phosphoryl group of G6P is crucial for efficient catalysis. Here we show that phosphonate analogues **1** and **2** can be oxidized by NtdC with ∼10% of the efficiency of the natural substrate as measured by second-order rate constants, comparable to the effect of replacement of the C5 oxygen atom with a methylene group. In addition, we have shown that NtdC-catalyzed oxidation of D-xylose proceeds at a rate that is 40000-fold lower than that of G6P, and the activity with xylose can be partially rescued by the addition of inorganic phosphite, improving the catalytic efficiency 4-fold. Taken together, we have been able to evaluate the role of the individual pieces of the $CH_2OPO_3^{2-}$ on the binding of G6P. Our results show that the electrostatic interactions of the phosphate, the bridging oxygen, and the substrate as a whole each contribute to the binding of the substrate in the active site. The resulting 3-keto products of these reactions are all substrates for the aminotransferase NtdA, and phosphite rescues NtdA-catalyzed 3-amino-3-deoxy-D-xylose transamination, reinforcing our observation that these two enzymes have co-evolved to process the relatively unstable 3-keto intermediate and minimize unproductive enolate formation. The ability of NtdC and NtdA to accept non-natural substrates such as carbocyclic and phosphonate analogues suggests that these enzymes could be used to produce novel and nonhydrolyzable kanosamine derivatives, which could in turn be incorporated into more complex natural product analogues with improved therapeutic properties.

ASSOCIATED CONTENT

Supporting Information

The Supporting Information is available free of charge at https://pubs.acs.org/doi/10.1021/acs.biochem.1c00283.

Full experimental procedures, including synthetic methods, protein purification, and kinetic methods, and supplemental figures and ^{1}H and ^{13}C NMR spectra of compounds synthesized in this study (PDF)

Accession Codes

NtdC, O07564; NtdA, O07566.

AUTHOR INFORMATION

Corresponding Author

David R. J. Palmer − *Department of Chemistry, University of Saskatchewan, Saskatoon, SK, Canada S7N 5C9;* orcid.org/0000-0001-9300-7460; Email: dave.palmer@usask.ca

Author

Natasha D. Vetter − *Department of Chemistry, University of Saskatchewan, Saskatoon, SK, Canada S7N 5C9;* orcid.org/0000-0002-0963-8858

Complete contact information is available at: https://pubs.acs.org/10.1021/acs.biochem.1c00283

Funding

This work was funded by an NSERC Discovery Grant to D.R.J.P. and an NSERC PGS award and University of Saskatchewan Gerhard Herzberg Memorial Fellowship to N.D.V.

Notes

The authors declare no competing financial interest.

ACKNOWLEDGMENTS

The authors thank K. Brown, P. Zhu, K. Fransishyn, K. Thoms, and other staff of the Saskatchewan Structural Sciences Centre for their expertise and D. Sanders for helpful discussions and shared equipment.

■ ABBREVIATIONS

3aX, 3-amino-3-deoxy-D-xylose; G6P, D-glucose 6-phosphate; G6PDH, G6P dehydrogenase; K6P, kanosamine 6-phosphate; 2KG, 2-ketoglutarate; 3oG6P, 3-oxo-D-glucose 6-phosphate; **3oX**, 3-oxo-D-xylose; 6PGDH, 6-phosphogluconate dehydrogenase; PGI, G6P isomerase; PGM, phosphoglucomutase.

■ REFERENCES

(1) Milner, J. L., Silo-Suh, L., Lee, J. C., He, H., Clardy, J., and Handelsman, J. (1996) Production of kanosamine by *Bacillus cereus* UW85. *Appl. Environ. Microbiol. 62*, 3061−3065.

(2) Janiak, A. M., and Milewski, S. (2001) Mechanism of antifungal action of kanosamine. *Med. Mycol. 39*, 401−408.

(3) Guo, J., and Frost, J. W. (2002) Kanosamine biosynthesis: A likely source of the aminoshikimate pathway's nitrogen atom. *J. Am. Chem. Soc. 124*, 10642−10643.

(4) Floss, H. G., Yu, T.-W., and Arakawa, K. (2011) The biosynthesis of 3-amino-5-hydroxybenzoic acid (AHBA), the precursor of mC7N units in ansamycin and mitomycin antibiotics: a review. *J. Antibiot. 64*, 35−44.

(5) Umezawa, S., Shibahara, S., Omoto, S., Takeuchi, T., and Umezawa, H. (1968) Studies on the biosynthesis of 3-amino-3-deoxy-D-glucose. *J. Antibiot. 21*, 485−491.

(6) Kevany, B. M., Rasko, D. A., and Thomas, M. G. (2009) Characterization of the complete zwittermicin a biosynthesis gene cluster from *Bacillus cereus*. *Appl. Environ. Microbiol. 75*, 1144−1155.

(7) Shafi, J., Tian, H., and Ji, M. (2017) *Bacillus* species as versatile weapons for plant pathogens: a review. *Biotechnol. Biotechnol. Equip. 31*, 446−459.

(8) Vetter, N. D., Langill, D. M., Anjum, S., Boisvert-Martel, J., Jagdhane, R. C., Omene, E., Zheng, H., van Straaten, K. E., Asiamah, I., Krol, E. S., Sanders, D. A. R., and Palmer, D. R. J. (2013) A previously unrecognized kanosamine biosynthesis pathway in *Bacillus subtilis*. *J. Am. Chem. Soc. 135*, 5970−5973.

(9) Boisvert-Martel, J. (2013) NtdB: A kanosamine-6-phosphate phosphatase. Ph.D. Thesis, University of Saskatchewan, Saskatoon, SK.

(10) Prasertanan, T., and Palmer, D. R. J. (2019) The kanosamine biosynthetic pathway in *Bacillus cereus* UW85: Functional and kinetic characterization of KabA, KabB, and KabC. *Arch. Biochem. Biophys. 676*, 108139.

(11) Fukui, S., and Hayano, K. (1969) Micro methods for determination of 3-ketosucrose and 3-ketoglucose. *Agric. Biol. Chem. 33*, 1013−1017.

(12) Hayano, K., Tsubouchi, Y., and Fukui, S. (1973) 3-Ketoglucose reductase of *Agrobacterium tumefaciens*. *J. Bacteriol. 113*, 652−657.

(13) Volc, J., Sedmera, P., Halada, P., Přikrylova, V., and Daniel, G. (1998) C-2 and C-3 oxidation of D-Glc, and C-2 oxidation of D-Gal by pyranose dehydrogenase from *Agaricus bisporus*. *Carbohydr. Res. 310*, 151−156.

(14) Kojima, K., Tsugawa, W., and Sode, K. (2001) Cloning and Expression of Glucose 3-Dehydrogenase from *Halomonas sp.* α-15 in *Escherichia coli*. *Biochem. Biophys. Res. Commun. 282*, 21−27.

(15) Vetter, N. D., and Palmer, D. R. J. (2017) Simultaneous Measurement of Glucose-6-phosphate 3-Dehydrogenase (NtdC) Catalysis and the Nonenzymatic Reaction of Its Product: Kinetics and Isotope Effects on the First Step in Kanosamine Biosynthesis. *Biochemistry 56*, 2001−2009.

(16) Vetter, N. D., Jagdhane, R. C., Richter, B. J., and Palmer, D. R. J. (2020) Carbocyclic Substrate Analogues Reveal Kanosamine Biosynthesis Begins with the α-Anomer of Glucose 6-Phosphate. *ACS Chem. Biol. 15*, 2205−2211.

(17) Tsang, W.-Y., Amyes, T. L., and Richard, J. P. (2008) A Substrate in Pieces: Allosteric Activation of Glycerol 3-Phosphate Dehydrogenase (NAD+) by Phosphite Dianion. *Biochemistry 47*, 4575−4582.

(18) Zhai, X., Malabanan, M. M., Amyes, T. L., and Richard, J. P. (2014) Mechanistic imperatives for deprotonation of carbon catalyzed by triosephosphate isomerase: enzyme activation by phosphite dianion. *J. Phys. Org. Chem. 27*, 269−276.

(19) Reyes, A. C., Zhai, X., Morgan, K. T., Reinhardt, C. J., Amyes, T. L., and Richard, J. P. (2015) The activating oxydianion binding domain for enzyme-catalyzed proton transfer, hydride transfer, and decarboxylation: Specificity and enzyme architecture. *J. Am. Chem. Soc. 137*, 1372−1382.

(20) Fernandez, P. L., Nagorski, R. W., Cristobal, J. R., Amyes, T. L., and Richard, J. P. (2021) Phosphodianion Activation of Enzymes for Catalysis of Central Metabolic Reactions. *J. Am. Chem. Soc. 143*, 2694−2698.

(21) Berkowitz, D. B., Bose, M., Pfannenstiel, T. J., and Doukov, T. (2000) α-Fluorinated phosphonates as substrate mimics for glucose 6-phosphate dehydrogenase: the CHF stereochemistry matters. *J. Org. Chem. 65*, 4498−4508.

(22) Blackburn, G. M., and Ingleson, D. (1978) Specific dealkylation of phosphonate esters using iodotrimethylsilane. *J. Chem. Soc., Chem. Commun.*, 870−871.

(23) Blackburn, G. M., and Ingleson, D. (1980) The dealkylation of phosphate and phosphonate esters by iodotrimethylsilane: a mild and selective procedure. *J. Chem. Soc., Perkin Trans. 1*, 1150−1153.

(24) Zygmunt, J., Kafarski, P., and Mastalerz, P. (1978) Preparation of Oxoalkanephosphonic Acids. *Synthesis 1978*, 609−612.

(25) Berkowitz, D. B., and Bose, M. (2001) (α-Monofluoroalkyl)-phosphonates: a class of isoacidic and "tunable" mimics of biological phosphates. *J. Fluorine Chem. 112*, 13−33.

(26) Adams, P. R., Harrison, R., Inch, T. D., and Rich, P. (1976) Dehydrogenation of the phosphonate analogue of glucose 6-phosphate by glucose 6-phosphate dehydrogenase. *Biochem. J. 155*, 1−4.

(27) Roach, D. J. W., and Harrison, R. (1981) Dehydrogenation by gluconate 6-phosphate dehydrogenase of an isosteric phosphonate substrate analogue. *Biochem. J. 197*, 731−735.

(28) Langill, D. M. (2010) Synthesis of neotrehalose; kinetics and mutagenesis of NtdC. Ph.D. Thesis, University of Saskatchewan, Saskatoon, SK.

(29) Ray, W. J., Long, J. W., and Owens, J. D. (1976) An analysis of the substrate-induced rate effect in the phosphoglucomutase system. *Biochemistry 15*, 4006−4017.

(30) Ray, W. J., and Long, J. W. (1976) Thermodynamics and mechanism of the PO_3 transfer process in the phosphoglucomutase reaction. *Biochemistry 15*, 3993−4006.

(31) Jencks, W. P., and Meister, A. (2006) Binding Energy, Specificity, and Enzymatic Catalysis: The Circe Effect. *Adv. Enzymol.*, 219−410.

https://doi.org/10.1021/acs.biochem.1c00283
Biochemistry 2021, 60, 1926−1932